View on Si(111)-(5×2)-Au with plasmon spectroscopy

Z. Mamiyev [*] and H. Pfnür [†]

Institut für Festkörperphysik, Leibniz Universität Hannover, Appelstraße 2, 30167 Hannover, Germany
and Laboratorium für Nano- und Quantenengineering (LNQE), Leibniz Universität Hannover,
Schneiderberg 39, 30167 Hannover, Germany

Si(111)-(5×2)-Au represents a prototype system for an adsorbate-induced spontaneous symmetry break by formation of quasi-one-dimensional atomic chains that are metallic. Surprisingly, the geometric structure of these chains is still under debate. In this paper, we show that examination of the unoccupied band structure by plasmon spectroscopy in combination with low energy electron diffraction contains sufficient information to discriminate between suggested models, favoring an optimal concentration of 6 atoms per (5×2) unit cell. Furthermore, we tested the stability of this structure and found that higher concentrations of Au tend to destabilize the single-domain structure on the slightly misoriented Si(111) surface, favoring formation of $(\sqrt{3} \times \sqrt{3})R30°$-ordered islands with a local concentration of 1 ML already at a surplus of 0.08 ML. The precise role of Au atoms at concentrations exceeding 0.60 ML that seem to stabilize formation of three domains, however, must remain open.

I. INTRODUCTION

Increasing structural and electronic correlations in reduced dimensions give rise to several physical phenomena that define the peculiarity of low-dimensional metallic systems [1–3]. One large family of such low-dimensional materials is the metal-induced atomic chains on semiconductor surfaces. Such wires can easily be produced by submonolayer metal deposition onto plane and stepped surfaces [4]. The resulting electronic properties of these atomic wires have been subject to intense fundamental studies and several exotic phenomena associated with ultimate smallness and dimensionality have been reported [2,5–7].

In particular, varying the concentration of adsorbed transition metal atoms on the Si(111) surface in the submonolayer range gives rise to apparent changes in the effective dimensionality of metal-induced surface structures from quasi-one (1D) to two dimensions (2D). As an example, Au forms (5×2), $(\sqrt{3} \times \sqrt{3})R30°$, and (6×6) reconstructions on this surface [8]. While most of them are clearly 2D, the (5×2) structure exhibits quasi-1D electronic states close to the Fermi level that disperse along the Au chains, as revealed by angle-resolved photoemission spectroscopy (ARPES) and by several other techniques [9–14]. No temperature-induced structural and/or electronic phase transitions have been observed down to 20 K for this phase [15], but due to its low symmetry, the Au-modified surface state shows a clear spin polarization that goes beyond the conventional Rashba-type spin-orbit interaction of Au [16]. Interestingly, the introduction of a regular array of steps by slight misorientation of the Si(111) surface (1°) leads, upon Au deposition, to formation of a

single (5×2) domain that can be destabilized to form all three domains by excess Au concentration, as we will show below.

In fact, although investigations of this system have a long history [17,18], the difficulties in determining absolute concentrations of an adsorbed material in the submonolayer regime is exemplarily demonstrated with this system. As a consequence, several structural models and optimal concentrations have been suggested for the (5×2) structure over time.

From early low energy electron diffraction (LEED) investigations an optimal Au concentration between 0.4 and 0.5 ML was proposed [11,19–22]. More recently, a comparison of scanning tunneling microscopy (STM) data and quantitative *ab initio* density functional theory (DFT) calculations [23] has led to the suggestion of an optimal concentration of 6 Au atoms per (5×2) unit cell, which corresponds to 0.6 ML. In this model [24] [the Erwin-Barke-Himpsel (EBH) model], the (5×2) structure consists of a single and a dimerized double-atomic Au chain, separated by a Si honeycomb chain (HC). According to the calculations, this structure is further stabilized by Si atoms adsorbed on the Au chain system. The existence of these Si adatoms as well as that of the Si-HC chain was corroborated by an optical reflection anisotropy study and DFT [25], which questioned the alternative model suggested by Abukawa *et al.* [26].

In contrast, Kwon and Kang proposed a model (called the KK model in the following) with an optimal Au concentration of 0.7 ML, i.e., one Au atom more per unit cell than in the EBH model [27]. With this model a metal-insulator transition, induced by adding additional Au to the optimal concentration, could successfully be modeled [15]. Similarly, many structural details seen with tunneling microscopy as well as electronic properties could be reproduced within this model [12]. Nevertheless, the optimal concentration suggested by this model is at variance with the findings of several recent

[*]mamiyev@fkp.uni-hannover.de
[†]pfnuer@fkp.uni-hannover.de

studies that found values for completion of the (5×2) structure between 0.60 and 0.67 ML [23,26,28,29]. In particular, the study by Kautz *et al.*, using low energy electron microscopy in combination with medium and high energy ion scattering, fixes this value to 0.65 ± 0.01 ML.

In view of these still controversial results, it is obvious that there is no generally accepted structural model for this system yet. While absolute calibrations of surface concentrations are generally very difficult, there may be alternative experimental approaches that are able to discriminate between the various models suggested. Indeed, as our results presented below demonstrate, testing the unoccupied band structure close to the Fermi level allows such a discrimination.

Indeed, plasmon spectroscopy has been found to reveal valuable information about the unoccupied band structure in low-dimensional systems [3,30] that is not easily accessible otherwise. Recently, localized plasmon polaritons have been investigated by IR-absorption spectroscopy on short sections of atomic wires on this surface [31], exploiting the fact that standing plasmonic waves have a finite energy at $k = 0$.

Therefore, complementing an older study [32], we employ plasmon spectroscopy to study the dispersion relation on single- and multiple-domain surfaces. We use electron energy loss spectroscopy with simultaneous high energy and high momentum resolution (EELS-LEED) to study the dispersion of the plasmonic loss induced by the Au chains. As we demonstrated recently [3,30,33], the close relationship between the unoccupied band structure, the edges of the electron-hole continuum, and the plasmon dispersion in quasi-1D systems [34] can directly be used for determination of the dispersion of unoccupied bands close to the Fermi level and for a comparison of calculated and experimental dispersions. This strategy is applied here in order to discriminate between band structures calculated from KK and EBH models. Moreover, we exploit the high sensitivity of this technique to chain ordering and confinement in the low-k regime to study the influence of disorder on wire length and structural arrangement [35,36].

Our paper is organized as follows: After the experimental section we first explain our coverage calibration and show the corresponding LEED pattern before concentrating on plasmon losses and their dispersion. Using established procedures, we calculate from this dispersion the upper edge of the electron-hole continuum, which for a single band crossing of the Fermi level is expected to coincide closely with the unoccupied band, and compare it with the calculated bands. In the second part, we study the effects of an increase of Au concentration beyond the optimal concentration, again with LEED and EELS-LEED, and finish with our summary and conclusions.

II. EXPERIMENTAL SETUP

The experiments were carried in a single UHV chamber which contains a LEED system dedicated to spot profile analysis (SPA-LEED), the spectrometer for high-resolution electron loss spectroscopy (EELS-LEED), and an ion-beam evaporator. It operates at a base pressure of 5×10^{-11} mbar. The electron energy loss spectrometer consists of electrostatic cylindrical analyzer and monochromator units that yield

12 meV energy resolution at the settings optimized for plasmon loss spectroscopy. The electrostatic deflection unit in front of the spectrometer allows us to scan the reciprocal space with a resolution of 0.01 Å^{-1}, thus combining high momentum resolution with high energy resolution (EELS-LEED) [37,38].

The Si(111) samples (size $5 \times 12 \times 0.3$ mm, $\rho_{Si(111)} \approx 0.01$ Ω cm, *n* doped) were oriented 1° away from (111) toward the $[\overline{1}\overline{1}2]$ direction with a precision of $\pm 0.1°$. This miscut allowed the formation of a single (5×2) domain.

Prior to sample installation in the UHV chamber, the sample was cleaned *ex situ* in petroleum benzene, acetone, and isopropanol. It was then degassed in vacuum at 600 °C for several hours followed by several flash-annealing cycles up to 1250 °C by direct current heating, while maintaining a pressure lower than 2×10^{-10} mbar. This procedure generates a well-defined (7×7) structure. DC current was always in the direction parallel to steps in order to avoid current-induced step bunching [39]. Gold evaporation was carried out at a sample temperature of 630 °C at a deposition rate of ~0.1 ML/min. After preparation, the sample was kept at this temperature for 20 s followed by a slow decrease of temperature to room temperature. Finally, the sample was annealed at 650 °C for ~5 s. Quartz microbalances (QMBs) were used to control the gold coverage. The density is given with respect to the Si layer density of the topmost plane (1 ML $\triangleq 7.83 \times 10^{14}$ atoms/cm^2). For calibration two QMBs were used, one at the sample position, another one on the evaporator. Taking the ratio of frequency changes (by fitting the slope) and the known mass-frequency relation of the quartz, the concentration of Au atoms on the sample surface was calculated [40]. For more accuracy, a SPA-LEED was used to control the surface quality following each preparation.

Prior to plasmon measurements different substrate temperatures and Au coverages were tested to optimize and prepare different surface structures. Thus single- and triple-domain structures without admixture of $\sqrt{3} \times \sqrt{3}$ were successfully prepared, as explained in more detail below.

For getting a good and precise estimate of the absolute Au concentration, we made reference to the Si(553)-Au system at its high-coverage phase. This phase at its completion has a gold concentration of 0.48 ML. Exceeding this concentration by more than 0.01 ML results in a significant decrease of plasmon energies [41]. At a surplus concentration of 0.03 ML the formation of a $\sqrt{3}$-ordered island was observed after annealing. Therefore, we used this system for further calibration of our quartz microbalances. Thus calibration with a precision of 0.01 ML was possible. For the investigations of the Si(111)-Au system, we worked with exactly the same setup and an identical geometry.

III. RESULTS AND DISCUSSION

A. Gold concentrations below and close to 0.6 ML

1. LEED

The samples after flash annealing to 1250 °C show the expected (7×7) pattern in LEED. Upon Au evaporation the (7×7) periodicity transforms into a single domain of a (5×2) structure, with a periodic spacing between wires of ~16 Å.
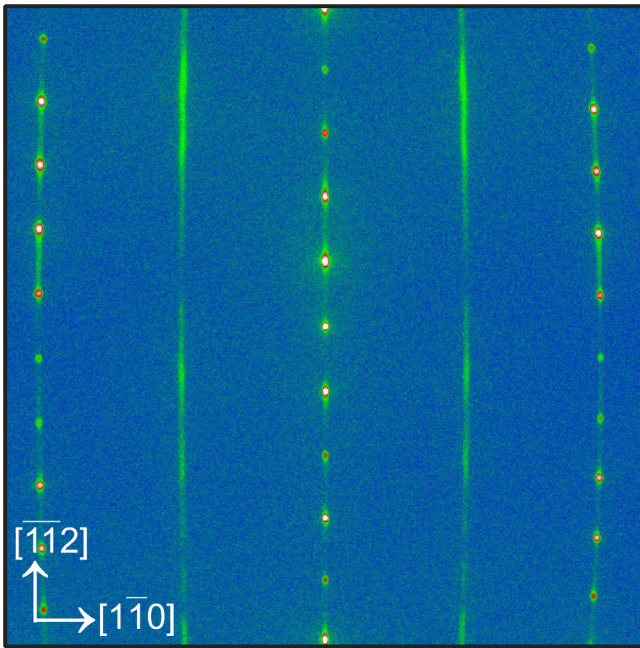
FIG. 1. Low energy electron diffraction pattern obtained for a Au concentration of 0.60 ML at 138 eV primary electron energy.
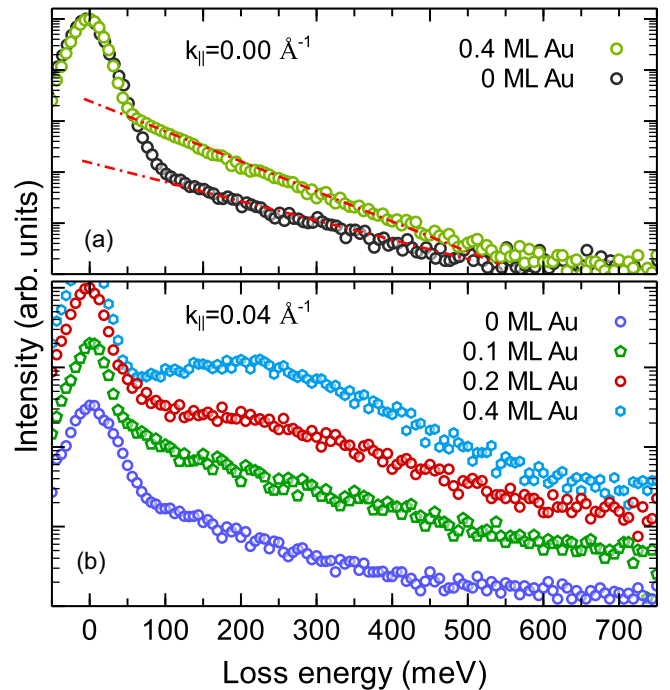

FIG. 2. Evolution of metallicity on the Si(111)-Au surface as a function Au deposition, as seen by EELS. Note the semilog scale. Spectra have been normalized to the elastic peak. (a) Change of Drude background upon Au deposition at $k_\parallel = 0$; (b) spectra recorded at $k_\parallel = 0.04$ Å^{-1} for the Au concentrations indicated. The evolution of the plasmonic loss associated with the formation of the (5×2) structure can clearly be seen at concentrations above 0.2 ML. In (b) the lowest three spectra are shifted against each other for better visibility.

The ×2 modulation along the wires is not correlated between wires so that only streaks are seen [15,32]. The ×2 periodicity along [1$\bar{1}$0] starts to appear at a Au concentration of 0.2 ML. Its intensity increases up to 0.6 ML Au coverage. On the other hand, the (7×7) structure loses intensity and finally disappears when the Au coverage approaches 0.6 ML. At the latter concentration the sharpest and most intense (5×2) structure was seen (see Fig. 1). Especially the ×2 intensity decreases quickly when the surface coverage is increased further.

This behavior gives evidence for the formation of (5×2)-ordered islands at Au concentrations above 0.2 ML, presumably with a local Au concentration close to the saturation of 0.60 ML, in coexistence with a low-density lattice gas that does not destroy the (7×7) structure of the clean Si(111) surface. These findings are in close agreement with those published earlier [22,29].

2. Plasmonic excitations

The growth mode with large (5×2)-ordered islands is corroborated by the evolution of loss intensities as a function of Au coverage, as shown in Fig. 2. Electron energy loss spectra (EELS) are shown there as a function Au concentration at $k_\parallel = 0$ and at $k_\parallel = 0.04$ Å^{-1}. At $k_\parallel = 0$ [Fig. 2(a)] no Au-induced loss features were detected, as expected. Only the structureless background increases significantly (please note the semilog scale) that follows closely an exponential dependence on k. This dependence is characteristic of metallic systems and is due to the continuum of low-energy electronic excitations [42] (please note that also the Si(111) surface has a metallic surface state with a low density of states [43]). This figure demonstrates that the metallicity of the Au covered Si(111) surface is fully developed at a Au concentration of 0.4 ML, i.e., at a concentration far below the saturation of the

(5×2) structure. Metallicity was indeed concluded also from angle-resolved photoemission experiments, in which a single nearly parabolic band was reported [10,44]. Indeed, as seen in Fig. 2(b), the evolution of the plasmonic loss starts already at a Au concentration above 0.2 ML. It is mainly the intensity of this loss that increases as a function of Au concentration with marginal shifts in the energetic position, in agreement with the assumption from above of phase coexistence between large islands of (5×2) and Si(111)-(7×7). Thus our results and earlier reports [44,45], which find the metallic states associated with anisotropic metallicity already at a Au coverage of 0.3 ML, are not at variance. They also agree with the results of Nagao *et al.* [45] for a nominal Au coverage of 0.44 ML for the same reason.

Momentum-resolved electron energy loss spectra at a Au concentration of 0.60 ML adsorbed on a freshly prepared surface are shown in Fig. 3. While a clear dispersing loss is seen in Fig. 3(a), i.e., along the [1$\bar{1}$0] direction parallel to the wires, no dispersing feature was found in the perpendicular direction shown in Fig. 3(b).

This anisotropic behavior of the dispersion is very similar to that observed in Au atomic wires on vicinal Si(111) surfaces at higher vicinal angles [3,30,46]. Therefore, we can safely associate the dispersing loss observed here with the quasi-1D plasmonic excitation of the Au wires in the (5×2) structure.
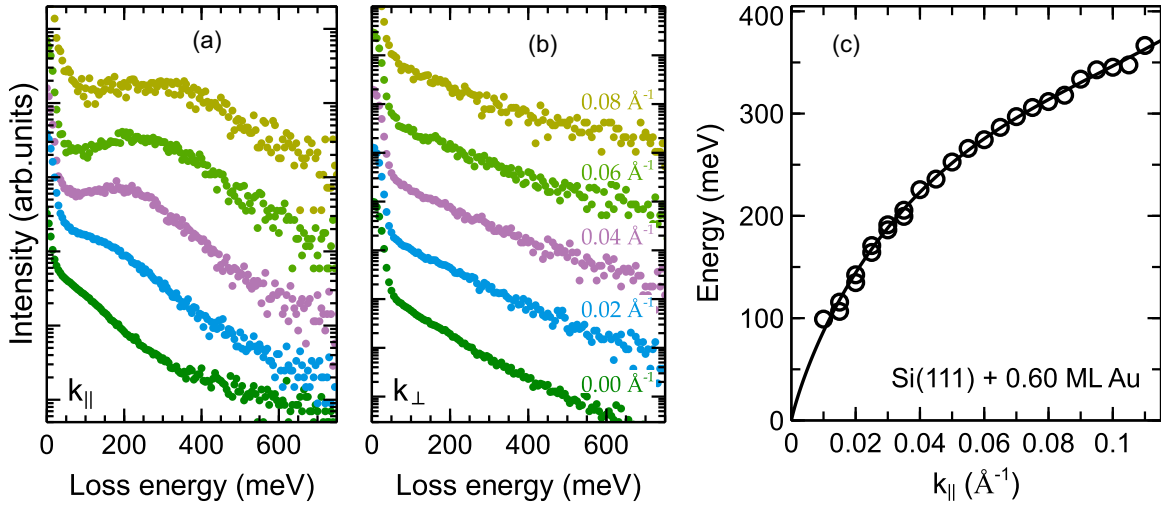
FIG. 3. Exemplary momentum-resolved loss spectra for Si(111)-Au surfaces recorded with a Au coverage of 0.60 ML. (a) Direction parallel to steps ($k_\parallel$) and (b) perpendicular to steps ($k_\perp$). (c) Dispersion of the plasmonic loss along [1$\bar{1}$0] determined from the loss maxima. The line is a fit with a nearly free electron gas (NFEG) model (electron density n) for a wire array of confining harmonic potentials of width a, wire separation d, effective electron mass m^*, and effective dielectric constant of the embedding environment ϵ. The fit parameters are $n = 1.46 \times 10^{-7}$ cm^{-1}, $m^* = 0.36 m_e$, $a = 5.8$ Å, $d = 16$ Å, $\epsilon = (11.5 + 1)/2$ [34]. While the fit is meant mainly as a guide to the eye, it also shows that the deviations from a NFEG are small in this case.

3. Comparison with theoretical models

For a quantitative comparison between plasmon dispersion and unoccupied band structure, the close relationship between the upper edge of the electron-hole continuum and the plasmon dispersion in quasi-1D systems is very helpful [30]. Here the quasi-1D array of wires is considered as a 2D electron gas that is confined to wires of finite width by a periodic confining potential [34]. The plasmon dispersion for these wires can be expressed as a function of the upper and lower boundary of the electron-hole continuum of excitations, ω_+ and ω_-, respectively. We use this relation for the determination of ω_+:

$$\omega_+(k_\parallel) = \sqrt{\frac{\omega_p^2(k_\parallel)(e^{A(k_\parallel)} - 1) + \omega_-^2(k_\parallel)}{e^{A(k_\parallel)}}} \quad (1)$$

with

$$A(k_\parallel) = \frac{2\pi \hbar^2 k_\parallel}{m^\star g_s V(k_\parallel)[1 - G(k_\parallel)]}.$$

$V(k)$ is the Fourier transform of the confining potential, $G(k)$ the local field correction factor due to electronic correlations, and g_s the spin degeneracy (1 or 2). As ω_p we insert the experimentally determined plasmon dispersion. ω_- was obtained from the Au-induced band below E_F in the calculated band structure of the EBH model, shown in Fig. 4(a), with the assumption that this band can be approximated by a parabola close to E_F. This assumption is not critical for the determination of the dispersion of ω_+, since ω_- has only a significant influence very close to E_F. Therefore, for the single band crossing E_F, ω_+ is expected to closely coincide with the unoccupied part of this band.

In Fig. 4 we compare our results of the unoccupied band dispersion derived from plasmon spectroscopy with the calculated band dispersions from Refs. [24,27]. Interestingly, an almost quantitative agreement is obtained between our

data and the undoped model of a Au-induced (5×1) structure of Erwin *et al.* [24] having a Au concentration of 0.6 ML. Only the experimental slope is slightly higher than in theory.

According to this model, the total energy can be lowered by adding Si adatoms [or just two electrons per (5×4) unit cell] onto the gold dimer chain. The existence of such adatoms has been verified by STM [12,23]. According to the calculations of Ref. [24], however, this type of doping leads to multiple openings of band gaps that are not compatible with our data, in which no indication for band gap opening is seen. Assuming that indeed the Si adatoms are necessary for stabilization of the structure, it seems that the effect of band gap opening, if
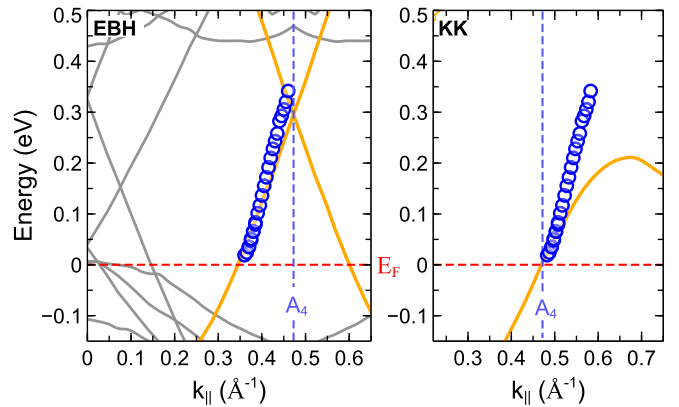

FIG. 4. Comparison of calculated electronic band structures (lines) with experiment (blue circles). The left panel shows the comparison with the EBH model [24] for the case of an undoped (5×1) structure, the right one that with the KK model [27]. The circles mark ω_+ determined from the plasmon dispersion shown in Fig. 3(c) (for details, see text).
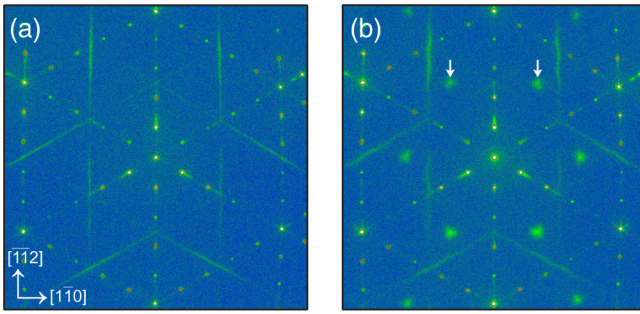
FIG. 5. LEED patterns after adsorption of 0.65 ML (a) and 0.70 ML of Au (b). Both coverages were annealed to 650 °C. The white arrows in (b) mark the $\sqrt{3}$ spots that appear at coverages above 0.68 ML.

any, is much less drastic than in the simulated EBH model. Alternatively, it may be that the (5×2) was formed without Si adatoms under our conditions of preparation. No systematic variation of preparation parameters has been performed, however, to answer this question.

Within the KK model [see Fig. 4(b)] band gaps in the unoccupied band structure are even larger than those calculated with the EBH model, which does not fit to our data. Since also the slope of the dispersion of the unoccupied band structure close to E_F is far off the experimental data points [see Fig. 4(b)], this model is clearly not able to describe our experimental findings.

While various mechanisms (lifetime broadening, finite k resolution, etc.) may make small band gaps invisible in plasmon spectroscopy, the trend within the EBH model to form a set of very flat bands with corresponding band gaps at large dimerizations lets us conclude that the dimerization leading to the ×2 modulation must be significantly smaller than that postulated by the model calculations, but this model is definitely compatible with our own estimate of the optimal Au concentration.

Although the ideal filling of a (5×2) can only be realized by an integer number of adatoms per unit cell, several experimental studies mentioned above obtained optimum coverages that correspond to noninteger numbers for ideal filling [28,29], indicating that there may be an important role to adatoms, as suggested theoretically [24]. We therefore investigated the role of additional Au exceeding the coverage of 0.60 ML up to 0.70 ML.

B. Au concentrations above 0.6 ML

When exceeding the Au concentration of 0.60 ML, the ×2 intensity in LEED is reduced, as already mentioned above. Furthermore, we detected a gradual reduction of stability of the single-domain structure and the appearance of all three domains. An example is shown in Fig. 5(a) at a concentration of 0.65 ML. Here the ×2 streaks of all three domains appear with still the original domain having the highest intensity, as shown in Fig. 5(a). In fact the intensity of the other domains becomes more pronounced upon preparation at 630 °C and subsequent postannealing at 650 °C for a few seconds. At this point, we can only speculate about possible reasons for
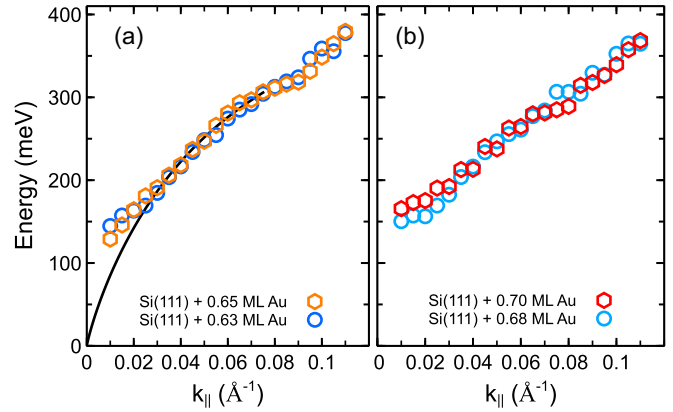

FIG. 6. Plasmon dispersion at concentrations above 0.60 ML. (a) Measured dispersion at 0.63 and 0.65 ML. For comparison (black line), the fit of the plasmon dispersion at a Au concentration of 0.60 ML of Fig. 3(c) is also shown. (b) Plasmon dispersions at 0.68 and 0.70 ML. The same domain orientation was recorded in all cases; i.e., measurements were along the [1$\bar{1}$0] direction.

the reduction of anisotropy in the formation of the (5×2) domains. Step decoration of Si steps by the surplus Au atoms [i.e., by Au atoms not needed for formation of (5×2)] may play a role, but also kinetic effects such as increased mobilities of steps and/or and easier diffusion of Au atoms at these higher Au concentrations.

When Au coverage is further increased, the formation of $\sqrt{3}$-ordered domains is observed, starting at a concentration of 0.68 ML, best seen after subsequent postannealing at 650 °C. An example at a Au concentration of 0.70 ML is shown in Fig. 5(b). The $\sqrt{3}$ structure has a local concentration of 1 ML [8]. In other words, there is a second range of coexistence at high Au coverages, now between (5×2) and $(\sqrt{3}×\sqrt{3})R30°$ phases, which is in agreement with published phase diagrams [22,29].

There is even quantitative agreement with respect to the critical concentration of phase coexistence between (5×2) and $(\sqrt{3}×\sqrt{3})R30°$ phases with Ref. [29]. We find the limit of stability of the pure phase of three domains of the (5×2) structure at a Au concentration of 0.67. Interestingly, this perfect agreement with Ref. [29] means that the anisotropy introduced by steps plays no role at all for this phase transition; i.e., at this concentration the single-domain structure is completely destabilized by surplus Au. For the pure three-domain structure (i.e., without appearance of $\sqrt{3}$ islands) the surface coverage to 0.65 ML and a preparation sample temperature of <630 °C turned out to be optimal. While this finding again agrees with previous results, it triggers some intriguing further questions about the role of adsorbed surplus Au atoms, which not only seem to destabilize the single-domain structure, but also to result in optimal stability of the single (5×2) phase with three domains. They cannot be resolved at this point.

In a second step, we compare the dependence of the plasmonic excitation and its dispersion on concentrations exceeding the Au coverage of 0.60 ML. This dependence turns out to be small, but with significant changes. When looking at Fig. 6(a), the increase of Au concentration from
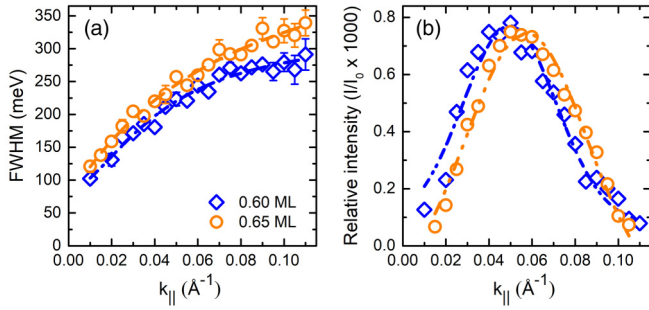
FIG. 7. (a) FWHM and (b) intensities of the plasmon loss, normalized to the elastic peak at $k_\parallel = 0$, both plotted as a function of $k_\parallel$ for Au coverages of 0.60 and 0.65 ML.

0.60 to 0.63 and 0.65 ML leaves the dispersion curve virtually unchanged. Only in the limit $k_\parallel \rightarrow 0$ is there a tendency for an increase of the energy values, as seen by the direct comparison with the 0.60 ML dispersion curve. This behavior has been observed before [35,36,47] and has been interpreted as being characteristic for increased disorder, as also seen in LEED. Disorder generally enhances scattering probabilities, also for plasmons, and can lead to the formation of standing waves with a finite wavelength [35,47]. In the simplest picture, this means that there is a maximum wavelength plasmons cannot exceed; i.e., dispersion ends at a finite average k value with a finite excitation energy close to $k_\parallel = 0$. As a consequence, this finite-energy value increases with the density of defects. In agreement with this interpretation, the deviation from the 0.60 ML dispersion curve gets larger at small $k_\parallel$ with increasing surplus Au concentration [see also Fig. 6(b)]. This interpretation of enhanced scattering probabilities is also supported by the observation of an increased half-width of the plasmon loss as a function of Au coverage, as shown in Fig. 7(a). An increased density of defects is expected to reduce the plasmonic lifetime, thereby increasing the linewidth of the plasmonic loss, as observed. Shorter wavelengths are more susceptible to defects, and indeed there is a tendency for the relative increase of the FWHMs to get bigger at large k.

At $k_\parallel$ values above 0.03 Å^{-1} the dispersion curves seem to be unchanged by excess Au apart from a small kink in the dispersion curve at a $k_\parallel$ value of 0.09 Å^{-1} [see Fig. 6(a)] that was not visible in the dispersion curve at 0.60 ML [cf. Fig. 3(c)]. This kink may indeed be an indication for opening of a small gap, which, contrary to the model with adsorbed Si atoms [24], is now caused by the adsorption of additional Au atoms.

This kink cannot be resolved anymore when the Au concentration is increased into the range of appearance of $\sqrt{3}$-ordered islands [Fig. 6(b)], possibly again due to the influence of enhanced disorder. These comparatively small changes of dispersion by increasing excess Au concentration indicate that extended islands with prevailing (5×2) order still exist, as also seen in LEED. The intensity of the plasmon loss, however, is reduced both by enhanced diffuse scattering due to disorder and by the formation of three domains. Both effects lead to enhanced uncertainties and an increased scatter of data.

No signs of an extra loss due to the $\sqrt{3}$-ordered islands was ever seen. Since also these islands form a 2D phase before at total coverages above 1 ML 3D islands can be formed [8] they are expected to exhibit a low-energy plasmon, if they were conducting. The absence of such a plasmon indicates that they are insulating.

Coming back to (5×2), the formation of three domains in a system with very limited order may also lead to crosstalk between the domains so that there is a possibility for crossover from quasi-1D to 2D. Although no plasmonic excitation was detected by us in the $k_\perp$ direction for Au concentrations up to 0.65 ML, interestingly, a weak absorption feature for the polarization perpendicular to chains was observed in IR experiments [15]. Similarly crossover from 1D to 2D was reported from ARPES experiments [44]. Some indication for such a behavior is the shift of the intensity maximum to higher $k_\parallel$ values, which corresponds to a redistribution of intensity in k space, and the widening of this maximum, as seen in Fig. 7(b). Also there an influence of disorder cannot be ruled out.

IV. SUMMARY AND CONCLUSIONS

In conclusion, we showed that the low-lying collective electronic excitations, here exemplified by the quasi-1D plasmons of the (5×2) phase of atomic Au wires on the Si(111) surface, can be directly used as a spectroscopy to obtain information about the unoccupied band structure close to the Fermi level. This part of the band structure turned out to be much more sensitive to differences between various structural models proposed for this system than spectroscopies of the occupied bands such as ARPES. Thus we were able to corroborate the validity of the EBH model that suggests a saturation coverage of 0.60 ML of Au, in agreement with our own coverage calibration and with our LEED investigations.

Furthermore, the combination of LEED and EELS yields detailed information about the growth modes of the (5×2) structure on this surface. It turns out that the whole range of Au concentrations from 0.2 ML up to 1 ML is governed mostly by phase coexistence of the (5×2) with either the clean Si(111)-(7×7) or with the ($\sqrt{3} \times \sqrt{3}$)$R30°$ phases, in agreement with earlier results on the phase diagram [29]. Only in a small concentration range around 0.60 ML does a single (5×2) phase exist.

The destabilization of the single-domain structure on this slightly stepped surface and the appearance of three domains at a Au concentration of 0.65 ML, which represents the concentration of maximum stability of the (5×2) structure on the flat surface with three domains, poses intriguing questions about the role of these "surplus" Au atoms. These questions must remain open at this point.

[1] J. Ortega and F. Himpsel, in *Very High Resolution Photoelectron Spectroscopy* (Springer, Heidelberg, 2007), pp. 147–183.

[2] P. C. Snijders and H. H. Weitering, Rev. Mod. Phys. **82**, 307 (2010).

[3] S. Sanna, T. Lichtenstein, Z. Mamiyev, C. Tegenkamp, and H. Pfnür, J. Phys. Chem. C **122**, 25580 (2018).

[4] F. Himpsel, K. Altmann, R. Bennewitz, J. Crain, A. Kirakosian, J. Lin, and J. McChesney, J. Phys.: Condens. Matter **13**, 11097 (2001).

[5] T. Lichtenstein, Z. Mamiyev, E. Jeckelmann, C. Tegenkamp, and H. Pfnür, J. Phys.: Condens. Matter **31**, 175001 (2019).

[6] L. Dudy, J. Aulbach, T. Wagner, J. Schafer, and R. Claessen, J. Phys.: Condens. Matter **29**, 433001 (2017).

[7] M. Tzschoppe, C. Huck, F. Hötzel, A. Butkevich, Z. Mamiyev, C. Ulrich, B. Günther, L. Gade, and A. Pucci, J. Phys.: Condens. Matter **31**, 195001 (2018).

[8] T. Nagao, S. Hasegawa, K. Tsuchie, S. Ino, C. Voges, G. Klos, H. Pfnür, and M. Henzler, Phys. Rev. B **57**, 10100 (1998).

[9] I. Collins, J. Moran, P. Andrews, R. Cosso, J. O'Mahony, J. McGilp, and G. Margaritondo, Surf. Sci. **325**, 45 (1995).

[10] R. Losio, K. N. Altmann, and F. J. Himpsel, Phys. Rev. Lett. **85**, 808 (2000).

[11] H. Kim, K. Shin, J. Ahn, and J. Chung, J. Korean Phys. Soc. **35**, S534 (1999).

[12] E. H. Do, S. G. Kwon, M. H. Kang, and H. W. Yeom, Sci. Rep. **8**, 1 (2018).

[13] J. N. Crain, M. C. Gallagher, J. L. McChesney, M. Bissen, and F. J. Himpsel, Phys. Rev. B **72**, 045312 (2005).

[14] J. L. McChesney, J. N. Crain, V. Pérez-Dieste, F. Zheng, M. C. Gallagher, M. Bissen, C. Gundelach, and F. J. Himpsel, Phys. Rev. B **70**, 195430 (2004).

[15] F. Hötzel, K. Seino, S. Chandola, E. Speiser, N. Esser, F. Bechstedt, and A. Pucci, J. Phys. Chem. Lett. **6**, 3615 (2015).

[16] K. Taguchi, K. Sumida, Y. Okuda, K. Miyamoto, A. Kimura, T. Oguchi, and T. Okuda, Phys. Rev. B **101**, 045430 (2020).

[17] H. Bishop and J. Riviere, J. Phys. D **2**, 1635 (1969).

[18] H. Lipson and K. Singer, J. Phys. C: Solid State Phys. **7**, 12 (1974).

[19] W. Święch, E. Bauer, and M. Mundschau, Surf. Sci. **253**, 283 (1991).

[20] L. D. Marks and R. Plass, Phys. Rev. Lett. **75**, 2172 (1995).

[21] Y. Nakajima, C. Voges, T. Nagao, S. Hasegawa, G. Klos, and H. Pfnür, Phys. Rev. B **55**, 8129 (1997).

[22] D. Grozea, E. Bengu, and L. Marks, Surf. Sci. **461**, 23 (2000).

[23] I. Barke, F. Zheng, S. Bockenhauer, K. Sell, V. V. Oeynhausen, K. H. Meiwes-Broer, S. C. Erwin, and F. J. Himpsel, Phys. Rev. B **79**, 155301 (2009).

[24] S. C. Erwin, I. Barke, and F. J. Himpsel, Phys. Rev. B **80**, 155409 (2009).

[25] C. Hogan, E. Ferraro, N. McAlinden, and J. F. McGilp, Phys. Rev. Lett. **111**, 087401 (2013).

[26] T. Abukawa and Y. Nishigaya, Phys. Rev. Lett. **110**, 036102 (2013).

[27] S. G. Kwon and M. H. Kang, Phys. Rev. Lett. **113**, 086101 (2014).

[28] N. McAlinden and J. F. McGilp, Europhys. Lett. **92**, 67008 (2010).

[29] J. Kautz, M. W. Copel, M. S. Gordon, R. M. Tromp, and S. J. van der Molen, Phys. Rev. B **89**, 035416 (2014).

[30] T. Lichtenstein, Z. Mamiyev, C. Braun, S. Sanna, W. G. Schmidt, C. Tegenkamp, and H. Pfnür, Phys. Rev. B **97**, 165421 (2018).

[31] F. Hötzel, K. Seino, C. Huck, O. Skibbe, F. Bechstedt, and A. Pucci, Nano Lett. **15**, 4155 (2015).

[32] C. Liu, T. Inaoka, S. Yaginuma, T. Nakayama, M. Aono, and T. Nagao, Phys. Rev. B **77**, 205415 (2008).

[33] Z. Mamiyev, S. Sanna, T. Lichtenstein, C. Tegenkamp, and H. Pfnür, Phys. Rev. B **98**, 245414 (2018).

[34] R. K. Moudgil, V. Garg, and K. N. Pathak, J. Phys.: Condens. Matter **22**, 135003 (2010).

[35] Z. Mamiyev, M. Tzschoppe, C. Huck, A. Pucci, and H. Pfnür, J. Phys. Chem. C **123**, 9400 (2019).

[36] Z. Mamiyev, S. Sanna, F. Ziese, C. Dues, C. Tegenkamp, and H. Pfnür, J. Phys. Chem. C **124**, 958 (2020).

[37] H. Claus, A. Büssenschütt, and M. Henzler, Rev. Sci. Instrum. **63**, 2195 (1992).

[38] T. Nagao and S. Hasegawa, Surf. Interface Anal. **30**, 488 (2000).

[39] Y. Homma and N. Aizawa, Phys. Rev. B **62**, 8323 (2000).

[40] G. Sauerbrey, Z. Phys. **155**, 206 (1959).

[41] Z. Mamiyev, C. Fink, S. Sanna, and H. Pfnür (unpublished).

[42] A. Liebsch, *Electronic Excitations at Metal Surfaces* (Springer, Boston, 1997).

[43] R. Losio, K. N. Altmann, and F. J. Himpsel, Phys. Rev. B **61**, 10845 (2000).

[44] K. N. Altmann, J. N. Crain, A. Kirakosian, J.-L. Lin, D. Y. Petrovykh, F. J. Himpsel, and R. Losio, Phys. Rev. B **64**, 035406 (2001).

[45] C. Liu, T. Inaoka, S. Yaginuma, T. Nakayama, M. Aono, and T. Nagao, Nanotechnology **19**, 355204 (2008).

[46] T. Nagao, G. Han, C. Hoang, J.-S. Wi, A. Pucci, D. Weber, F. Neubrech, V. M. Silkin, D. Enders, O. Saito, and M. Rana, Sci. Technol. Adv. Mater. **11**, 054506 (2010).

[47] Z. Mamiyev, T. Lichtenstein, C. Tegenkamp, C. Braun, W. G. Schmidt, S. Sanna, and H. Pfnür, Phys. Rev. Mater. **2**, 066002 (2018).